PRAMANA — journal of physics

Vol. 79, No. 6
December 2012
pp. 1443–1456

Influence of pseudorandom bit format on the direct modulation performance of semiconductor lasers

MOUSTAFA AHMED[1,2,*], SAFWAT W Z MAHMOUD[2] and ALAA A MAHMOUD[2]

[1]Department of Physics, Faculty of Science, King Abdulaziz University, M.B. 20803, Jeddah 21589, Saudi Arabia
[2]Department of Physics, Faculty of Science, Minia University, 61519 El-Minia, Egypt
*Corresponding author. E-mail: mostafa.hafez@science.miniauniv.edu.eg

MS received 13 January 2012; revised 29 April 2012; accepted 29 May 2012

Abstract. This paper investigates the direct gigabit modulation characteristics of semiconductor lasers using the return to zero (RZ) and non-return to zero (NRZ) formats. The modulation characteristics include the frequency chirp, eye diagram, and turn-on jitter (TOJ). The differences in the relative contributions of the intrinsic noise of the laser and the pseudorandom bit-pattern effect to the modulation characteristics are presented. We introduce an approximate estimation to the transient properties that control the digital modulation performance, namely, the modulation bit rate and the minimum (setting) bit rate required to yield a modulated laser signal free from the bit pattern effect. The results showed that the frequency chirp increases with the increase of the modulation current under both RZ and NRZ formats, and decreases remarkably with the increase of the bias current. The chirp is higher under the RZ modulation format than under the NRZ format. When the modulation bit rate is higher than the setting bit rate of the relaxation oscillation, the laser exhibits enhanced TOJ and the eye diagram is partially closed. TOJ decreases with the increase of the bias and/or modulation current for both formats of modulation.

Keywords. Chirp; digital modulation; eye diagram; jitter; semiconductor laser; simulation.

PACS Nos 42.55.Px; 42.60.Mi; 07.05.Tp

1. Introduction

Direct modulation is a typical advantage of semiconductor lasers, which makes them suitable in many communication systems in which they directly convert electrical signals into optical ones with frequencies reaching several GHz. The variety of nonlinear phenomena in the semiconductor laser operation makes the laser behaviour under high-speed modulation an interesting and important subject of study. The nonlinear coupling between the injected carriers in the active region of a semiconductor laser and the emitted

DOI: 10.1007/s12043-012-0349-7; ***e*Publication: 30 August 2012**

photons is characterized by relaxation oscillations in the transient regime of the laser. These relaxation oscillations set an upper limit to the modulation bandwidth [1–3]. In addition, the relaxation oscillations delay for a turn-on time, which is the time interval between the onset of the electrical pulse and the resulting optical pulse. The intrinsic noise of the laser, which originates from the inclusion of the spontaneous emission into the lasing mode and electron–hole recombination processes [4,5], makes the turn-on time a randomly fluctuating quantity [6]. Moreover, in digital transmission systems the laser is subjected to direct digital modulation by pseudorandom 'ON-OFF keying', which adds to fluctuations of the turn-on time giving rise to jitter. This turn-on jitter (TOJ) is an important aspect of communication systems that measures degradation of the system performance [7]. TOJ is defined as the standard deviation of the random turn-on delay time [8]. The digital modulation performance of the semiconductor laser is controlled also by the maximum modulation bit rate of the laser and the setting time of the relaxation oscillation. Gustavsson *et al* [9] and Ahmed *et al* [8] pointed out that when the laser is modulated by pseudorandom bit stream with the bit slot being shorter than the setting time of relation oscillation, the modulated laser signal depends on the history of the '1' bits preceding every '0' bit; a phenomenon known as 'bit-pattern effect'. This bit-pattern effect is enhanced under high speed modulation and results in large values of TOJ [8], which accounts for the deterioration of the modulation performance of the laser. Both the turn-on delay time and setting time of the relaxation oscillations depend on the injection current [8,10]. Evaluation of the roles played by the turn-on delay time and setting time of the relaxation oscillations to the digital modulation characteristics of the semiconductor laser is essential to improve the laser modulation performance.

The intensity modulation of semiconductor lasers is associated also with phase modulation due to the large value of the linewidth enhancement (α) factor [4]. The modulating current source of the laser modulates the injected carriers in the active layer also, which causes variation in the refractive index and lasing frequency. This frequency variation is referred to as frequency chirping. Under large-signal modulation, chirping represents a form of intrinsic phase modulation thus broadening the line shape [11] and limiting the transmission distance of high rate systems [12,13]. Semiconductor lasers are characterized by two types of chirp. The first type is the transient or peak-to-peak chirp, which originates from relaxation oscillations that cause transient fluctuations in the effective refractive index of the active layer and the carrier density [14]. The other type is the adiabatic chirp, which is induced when the laser reaches its steady state and the frequency fluctuates around mean values in both '1' and '0' states [14].

On the other hand, an important issue in designing a digital optical communication system is to decide how the electrical signal can be converted into an optical bit stream. There are two common techniques to represent information in a binary electrical pulse train; the RZ and NRZ formats. The NRZ modulation format has been used extensively in many data communication systems mainly because of its relative ease of generation [7]. Another reason is that the signal bandwidth of an NRZ pulse train is about 50% smaller than that of an RZ pulse train [15]. The RZ format uses only half the bit duration for data transmission and therefore it requires twice the bandwidth of NRZ coding [16]. Most of the previous studies concentrated on the digital modulation characteristics of semiconductor lasers using a NRZ modulation format, but very limited reports compared the modulation performance under both formats [16–18]. Such comparison

is a prerequisite for exploring a better code for achieving higher digital modulation performance especially under gigabit-per-second bit rates.

In this paper, we introduce numerical simulations of the modulation characteristics of semiconductor lasers subjected to RZ and NRZ pseudorandom bit formats with gigabit-per-second rates. The simulations are based on large-signal model of the laser rate equations. The modulation performance is determined in terms of the signal power, frequency chirp, TOJ and the quality of the eye diagram. The eye diagram is constructed by dividing the modulated laser waveform into segments of two-bit length and overlaying each on to others. The degree of eye opening is evaluated in terms of a laser signal Q-factor which defines the difference between the average intensities in the '1' and '0' states relative to summation of the corresponding standard deviations [7]. We approximately estimate the maximum modulation bit rate and the bit-pattern effect-free bit rate (setting bit rate) from the laser transients and explore their influence on the modulation performance. Comparison of the simulated results under RZ and NRZ modulation formats is given over wide ranges of bias and modulation currents.

The paper is constructed as follows. In the following section, the simulation model of laser dynamics under digital modulation is introduced. Section 3 presents procedures of numerical calculations. In §4, the results of numerical simulations of laser characteristics under RZ and NRZ pseudorandom bit formats with gigabit-per-second rates are given. Conclusions of the present work appear in §5.

2. Simulation model of semiconductor laser dynamics under digital modulation

The dynamics of semiconductor lasers subjected to pseudorandom digital modulation are described by the following stochastic rate equations of the electron number injected into the active layer $N(t)$, emitted photon number $S(t)$ and optical phase $\theta(t)$ [5]:

$$\frac{\mathrm{d}N}{\mathrm{d}t} = \frac{1}{e}I(t) - AS - \frac{N}{\tau_s} + F_N(t), \tag{1}$$

$$\frac{\mathrm{d}S}{\mathrm{d}t} = (G - G_{\mathrm{th}})S + \frac{a\xi}{V}N + F_S(t), \tag{2}$$

$$\frac{\mathrm{d}\theta}{\mathrm{d}t} = 2\pi\delta v(t) = \frac{\alpha a\xi}{2V}(N - \bar{N}) + F_\theta(t), \tag{3}$$

where G is the optical gain (per second) which is described by the nonlinear form [19]:

$$G = A - BS, \tag{4}$$

where A and B are the linear and nonlinear (suppressed) gain coefficients. They are given by

$$A = \frac{a\xi}{V}(N - N_g) \tag{5}$$

$$B = \frac{9}{2}\frac{\pi c}{\varepsilon_0 n_r^2 \hbar\lambda_0}\left(\frac{\xi\tau_{\mathrm{in}}}{V}\right)^2 a\,|R_{cv}|^2\,(N - N_s). \tag{6}$$

In the above equations, a is the tangential gain coefficient, ξ is the confinement factor of the electric field to the active region whose volume is V and refractive index is n_r, λ_0 is the emission wavelength, $\hbar$ is the reduced Planck's constant, c and ε_0 are the speed of light and permittivity in vacuum, N_g is the electron number at transparency, τ_{in} is the electron intraband relaxation time, N_s is an electron number characterizing the nonlinear gain, R_{cv} is the dipole moment, e is the electron charge, and τ_s is the electron lifetime due to spontaneous emission. G_{th} represents the threshold gain level. In eq. (3), $\Delta v(t)$ is the frequency chirp associated with the time variation of the optical phase $\theta(t)$, α is the linewidth enhancement factor and $\bar{N}$ is the time average value of $N(t)$.

The current term of eq. (1) varies with time as

$$I(t) = I_{\text{b}} + I_{\text{m}}\Psi(t), \tag{7}$$

where the time varying function $\Psi_{\text{m}}(t)$ has either '0' or '1' level describing the binary bit format of the modulating current; it commonly describes either RZ or NRZ pseudorandom bit generation. The speed of this time variation is determined by the bit rate $B = 1/T_{\text{b}}$, with T_{b} representing the bit duration. The bit slot of the NRZ bit pattern is equal to the bit duration T_{b}, whereas the bit slot of the RZ bit pattern is set to be half of T_{b}. In eqs (1)–(3), the terms $F_N(t)$, $F_S(t)$, and $F_\theta(t)$ are Langevin noise sources describing the intrinsic fluctuations in $N(t)$, $S(t)$ and $\theta(t)$, respectively, associated with quantum transitions of electrons between the valence and conduction bands in the absorption, spontaneous emission and stimulated emission processes [4,5]. These noise sources represent white noise with Gaussian statistics and are δ-correlated [5],

$$\langle F_a(t)F_a(t')\rangle = V_{aa}\delta(t-t'), \quad a = S, N \text{ or } \theta, \tag{8}$$

$$\langle F_S(t)F_N(t')\rangle = V_{SN}\delta(t-t'), \tag{9}$$

$$\langle F_S(t)F_N(t')\rangle = V_{SN}\delta(t-t'), \tag{10}$$

$$\langle F_S(t)F_\theta(t')\rangle = 0, \tag{11}$$

$$\langle F_N(t)F_\theta(t')\rangle = V_{N\theta}\delta(t-t'), \tag{12}$$

where the coefficients V_{ab}, with a and b being S, N or θ, are the correlation coefficients. It is worth noting that rate eq. (3) of $\theta(t)$ is coupled to eq. (1) of $N(t)$ and eq. (2) of $S(t)$ through the above cross-correlations of the noise sources.

3. Numerical calculations

Equations (1)–(3) are coupled first-order differential equations, and are solved numerically by means of the fourth-order Runge–Kutta method [20] assuming rectangular pulses of the modulating current in eq. (4). In rate eq. (1), the processes of carrier pumping and recombination operate on a time-scale of nanoseconds, while in rate eq. (2) the processes of stimulated and spontaneous emission and photon loss operate on a time-scale of picoseconds. The integration step Δt is chosen to be within the scale of the faster processes of photon emission and absorption, $\Delta t = 2$ ps. The time range $\Delta t = 1$–5 ps was found to result in stable solution of the rate equations. The time step of integration is set

as short as 2 ps. The laser is modulated with RZ and NRZ pseudorandom bit streams of word length 2^{15}–1 in order to collect significant statistics of modulation characteristics. The pseudorandom bit stream is generated by the uniformly distributed random number generations of the computer; random values less than 0.5 are converted to zero and other values are converted to unity. The modulation characteristics are simulated as functions of the bias current $I_{\rm b}$ and modulation current $I_{\rm m}$. The modulation bit rate is set to be $B = 2.5$ Gbps. The present numerical calculations are applied to InGaAsP lasers emitting at wavelength $\lambda = 1.55$ μm as the most popular light source in optical fibre communication systems. The non-radiative recombination processes are taken into account in the rate equation through the lifetime τ_s as

$$\frac{1}{\tau_s} = B_{\rm eff}\frac{N}{V}, \tag{13}$$

where $B_{\rm eff}$ is the effective rate of electron recombination consisting of both the radiative and non-radiative recombination processes. Typical values of the parameters of these lasers are listed in table 1. The Langevin noise sources $F_N(t)$, $F_S(t)$ and $F_\theta(t)$ in eqs (1)–(3) are generated at instant t_i of integration as [5]

$$F_S(t_i) = \sqrt{\frac{V_{SS}(t_i)}{\Delta t}}\,g_S, \tag{14}$$

$$F_\theta(t_i) = \frac{1}{S(t_i-1)+1}\sqrt{\frac{V_{SS}(t_i)}{\Delta t}}\,g_\theta, \tag{15}$$

$$F_N(t_i) = \sqrt{\frac{V_{NN}(t_i)+2k_S(t_i)V_{NS}(t_i)}{\Delta t}}\,g_N - k_S(t_i)\{F_S(t_i)+2[S(t_{i-1})+1]F_\theta(t_i)\}, \tag{16}$$

where the correlation coefficients are determined from $S(t_{i-1})$ and $N(t_{i-1})$ as

$$V_{SS}(t_i) = 2\frac{a\xi}{V}\,[S(t_{i-1})+1]\,N(t_{i-1}), \tag{17}$$

Table 1. Typical values of the parameters of a 1.55-μm InGaAsP laser.

Symbol	Meaning	Value	Unit
a	Tangential gain coefficient	7.85×10^{-12}	$\rm s^{-1}$
ξ	Field confinement factor	0.2	–
V	Volume of the active region	60	$\mu\rm m^3$
L	Length of the active region	250	μm
n_r	Refractive index of the active region	3.56	–
N_g	Electron number at transparency	5.31×10^{7}	–
α	Linewidth enhancement factor	4	–
$\tau_{\rm in}$	Electron intraband relaxation time	0.13	ps
$\lvert R_{\rm cv}\rvert^2$	Squared absolute value of the dipole moment	9.53×10^{-57}	$\rm C^2m^2$
N_s	Electron number characterizing nonlinear gain	4.05×10^{7}	–
$B_{\rm eff}$	Effective rate of non-radiative recombination	3.9×10^{-16}	$\rm s^{-1}$
$G_{\rm th}$	Threshold gain level	8.84×10^{10}	$\rm s^{-1}$

$$V_{NN}(t_i) = 2\left[\frac{1}{\tau_s} + \frac{a\xi}{V}S(t_{i-1})\right]N(t_{i-1}), \tag{18}$$

$$V_{NS}(t_i) = -\frac{a\xi}{V}N(t_{i-1})[S(t_{i-1}) + 1] + N_g S(t_{i-1}), \tag{19}$$

$$k_S(t_i) = -\frac{V_{NS}(t_i)}{V_{SS}(t_i)}. \tag{20}$$

In the above equations, g_S, g_θ and g_N are three independent Gaussian random numbers with means of zero and variances of unity [5].

The digital modulation performance of the laser is evaluated in terms of the time trajectory of the modulated laser signal, frequency chirp, eye diagram and the associated values of TOJ and Q-factor of the laser signal, Q_{signal}. The eye diagram is constructed by dividing the stream of $P(t)$ into 2-bits-long sequences and overlying each onto others. In this case of pseudorandom bit modulation, τ_{on} in each '1' bit is defined as the time at which the power in the '1' bit preceded by '0' bit(s) first surpasses 50% of the summation of the steady-state powers corresponding to the bias and modulation currents [8]. TOJ is the standard deviation of the fluctuations in τ_{on}. Q_{signal} is a characteristic quantity analogous to the Q-factor that characterizes the eye diagram in optical fibre communication systems [7], and is defined as [8]

$$Q_{\text{signal}} = \frac{\bar{P}_1 - \bar{P}_0}{\sigma_0 + \sigma_1}, \tag{21}$$

where $\bar{P}_j$ and σ_j, with $j = 0$ or 1, are the time average of the power and the standard deviation of the corresponding fluctuations in either signal level, respectively. $\bar{P}_j$ at the on, $j = 1$, or off, $j = 0$, level of the laser signal emitted from the front facet is calculated from the corresponding time-average number of the emitted photons $\bar{S}_j$ as

$$\bar{P}_j = \frac{hvc}{2n_a L}\frac{(1 - R_f)\ln(1/R_f R_b)}{\left(1 - \sqrt{R_f R_b}\right)\left(1 - \sqrt{R_f R_b}\right)}\bar{S}_j, \quad j = 0, 1, \tag{22}$$

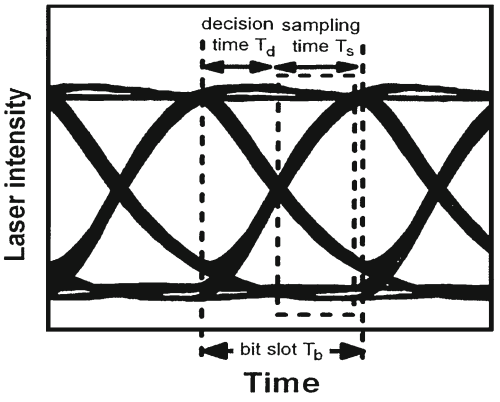

Figure 1. Illustrative figure of a three-bit-long eye diagram indicating the sampling and decision times.

where n_a and L are the refractive index and length of the active region, respectively, hv is the photon energy of the emitted light, and R_f and R_b are the power reflectivities of the front and back facets, respectively.

Q_{signal} is used to determine the most open portion of the eye diagram over which the signal has optimum characteristics. This goal is achieved by following a technique similar to that proposed by Ahmed *et al* [8]. The eye diagram is divided into 10 sampling periods, each of length equal to $T_s = 0.1T_b$ under the NRZ modulation and $T_s = 0.05T_b$ under the RZ modulation, and determining the corresponding value of Q_{signal} over each sampling period. Each sampling period corresponds to a different decision time in the range $0 < T_d \leq T_b - T_s$, as shown in figure 1. The section of maximum opening of the eye is then of duration T_s and corresponds to the decision time T_d at which Q_{signal} is maximum.

4. Results and discussion

4.1 *Transient guides to the maximum bit rate (B_{max}) and setting bit rate ($B_{setting}$)*

Before discussing simulation results of laser modulation, we seek approximated estimations of the maximum bit rate B_{max} of digital modulation of the laser at given bias and modulation currents as well as the corresponding setting bit rate $B_{setting}$ required to yield a modulated signal free of bit-pattern effects. This is done by examining the time variation of the photon number $S(t)$ during the transient regime of the laser. The noise sources in eqs (1)–(3) are ignored for such calculations. In this case neither $S(t)$ nor $N(t)$ depends on the phase $\theta(t)$, as given in eqs (1) and (2). Therefore, in this subsection we numerically solve only rate eqs (1) and (2) without the noise sources $F_N(t)$, $F_S(t)$. By exciting the laser with a rectangular current pulse, we calculate the turn-on delay time τ_{on} and setting time of the relaxation oscillations $t_{setting}$ at which the transients die away. We estimate the maximum modulation bit rate B_{max} as $1/\tau_{on}$, and estimate the reciprocal of $t_{setting}$ as the setting bit rate $B_{setting}$. The estimated values of B_{max} and $B_{setting}$ are plotted in figures 2a and b as functions of the bias current I_b and modulation current I_m. Figure 2a shows that B_{max} increases with the increase of I_b and/or I_m. As found numerically, B_{max} increases from 5 to 11.11 Gbps when $I_b = 1.5I_{th}$ while I_m increases from 0.2 to $4I_{th}$. Also, B_{max}

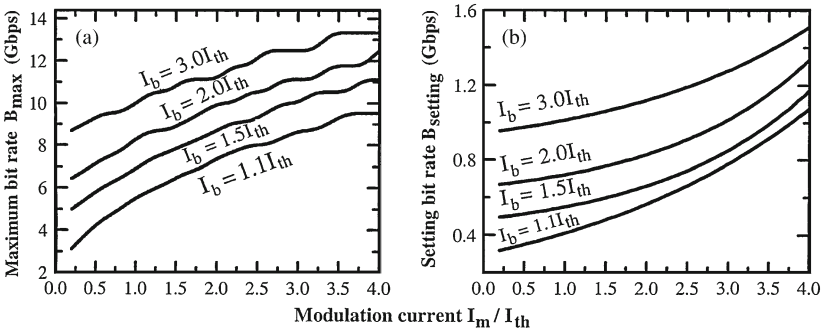

Figure 2. Variation of (**a**) $B_{setting}$ and (**b**) B_{max} with I_b and I_m.

increases from 9 to 13.33 Gbps when I_m =4.0I_{th} while I_b increases from 1.1 to 3I_{th}. Figure 2b shows that $B_{setting}$ increases monotonically with the increase of I_b and/or I_m. It increases from 490 Mbps to 1.17 Gbps with the increase of I_m from 0.2 to 4I_{th} when I_b =1.5I_{th}, whereas it increases from 1.07 to 1.5 Gbps when $I_m = 4I_{th}$.

4.2 *Laser waveform and frequency chirp*

Examples of the modulated signal and frequency chirp are shown in figures 3a and b, which correspond to $I_m = 2I_{th}$ and $B = 2.5$ Gbps under (a) NRZ and (b) RZ formats, respectively. The waveforms of the NRZ format display, in both the ON and OFF states, the relaxation oscillations that characterize the laser transients when the current level is above the threshold current I_{th}. The relaxation oscillations are associated with inferior properties such as turn-on and turn-off delays in the '1' and '0' bits that follow opposite bits. Both τ_{on} and the steady-state value of the fluctuating power are different in the displayed windows of '1' bit(s), which count to random fluctuations of these characteristics over the entire waveform. The dispersion associated with fluctuations in τ_{on} determines the TOJ, which then originates from both the intrinsic noise and the pseudorandom sequence of bits preceding each '1' bit in the modulation bit pattern. The waveforms of the RZ format in figure 3b show similar behaviours of the waveforms except that the waveform does not continue over every '1' bit, but drops to zero at the middle of the bit duration T_b. The short bit slot of $T_b/2 = 1/(1.25\ \text{Gbps}) = 0.25$ ns allows only for setting the first overshoot of the relaxation oscillations in the '1' bits. The different heights of these overshoots are manifestations of the pseudorandom nature of the RZ-bit format.

On the other hand, as the laser current changes from the OFF state to the ON states, the carrier number abruptly changes, resulting in transient variations of the optical phase $\theta(t)$, i.e., in the frequency shift $\delta v(t)$ (chirp) [14], as shown in the lower plots of figure 3. This frequency chirp represents a form of intrinsic phase modulation that broadens the laser lineshape [11]. As seen in the plots of $\delta v(t)$, the leading and trailing edges of the pulse have different carrier frequencies, which form the transient or peak-to-peak chirp [14]. This transient chirp originates from the relaxation oscillations, which cause transient fluctuations in the effective refractive index of the active layer. When the laser reaches

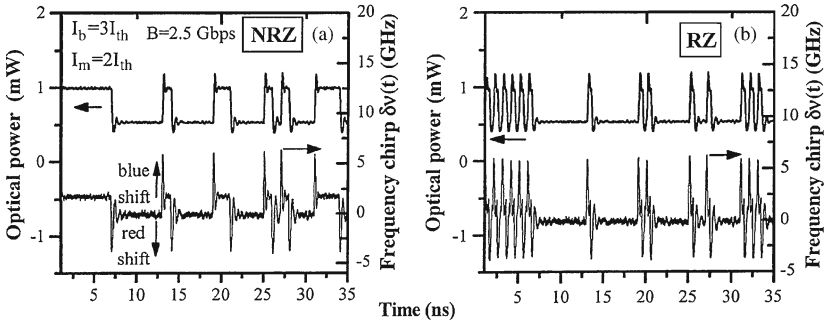

Figure 3. Laser signal power and chirp when $I_b = 3I_{th}$ and $I_m = 2I_{th}$ under (**a**) NRZ and (**b**) RZ modulations.

its steady state, the frequency chirp fluctuates around mean values in both '1' and '0' states. The frequency difference between the '1' and '0' states gives rise to the adiabatic chirp [14]. Figure 3a shows that the frequency chirp of the output pulse undergoes a blue-shift ($\delta v = 4.796$ GHz) during the rising edge and a red-shift ($\delta v = -3.82$ GHz) during the trailing edge under the NRZ modulation, whereas under the RZ modulation the frequency undergoes a blue-shift ($\delta v = 4.76$ GHz) during the rising edge and a red-shift ($\delta v = -3.78$ GHz) during the trailing edge as shown in figure 3b.

Figures 4a and b show variations of the peak-to-peak chirp with I_m under both RZ and NRZ modulation when $I_b = 1.5I_{th}$ and $3I_{th}$, respectively. Figure 4a shows that under both the NRZ and RZ formats (but up to $I_m = 2.5I_{th}$), the peak-to-peak chirp increases with the increase in I_m, which can be interpreted as follows. The increase of I_m results in an increase of the intensity of '1' level, which then enlarges the blue-shift. The figure shows also that under the RZ modulation format when $I_m > 2.5I_{th}$, the chirp becomes almost constant at 34.5 GHz. The overall range of the peak-to-peak frequency chirp under the RZ modulation format (13.44–34.88 GHz) is wider than that (12.56–29.41 GHz) under the NRZ modulation format, which indicates that the NRZ scheme has a better-defined central frequency compared to the RZ scheme. Balle *et al* [17] attributed this result to the fact that under the NRZ modulation, half of the '1' bits, on the average, are preceded by similar '1' bits, and then have no chirp. Figure 4b shows similar results when I_b increases to $3I_{th}$. Up to $I_m = 1.25I_{th}$, the RZ peak-to-peak frequency chirp values are larger than those of the NRZ peak-to-peak frequency chirp. Above this modulation current, the chirp becomes almost similar. That is, the NRZ scheme has a better-defined central frequency compared to the RZ scheme in low range of I_m but exhibits almost similar behaviour in the high range of I_m. Comparing with the results in figure 4a of $I_b = 1.5I_{th}$, a noticeable reduction of δv is seen in both the formats, which confirms the improvement of the modulation performance by increasing I_b.

4.3 *Eye diagram analysis*

The eye diagram is used to examine the quality of the modulated laser signal including the random phenomenon of the turn-on delay. Figure 5 illustrates evolution of the eye diagram under the NRZ modulation with the increase of the bit rate B while I_b and I_m

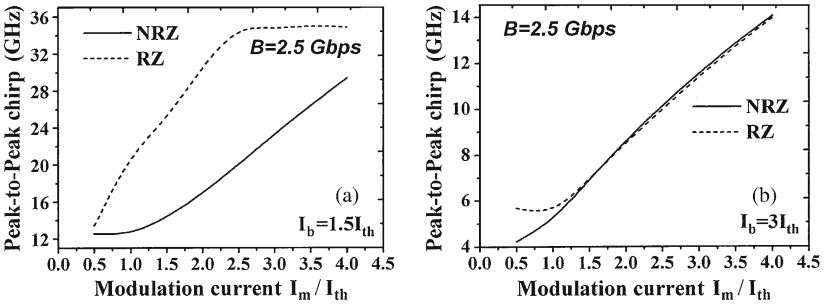

Figure 4. Variation of laser chirp with I_m when (**a**) $I_b = 1.5I_{th}$ and (**b**) $I_b = 3I_{th}$ under both RZ and NRZ modulations.

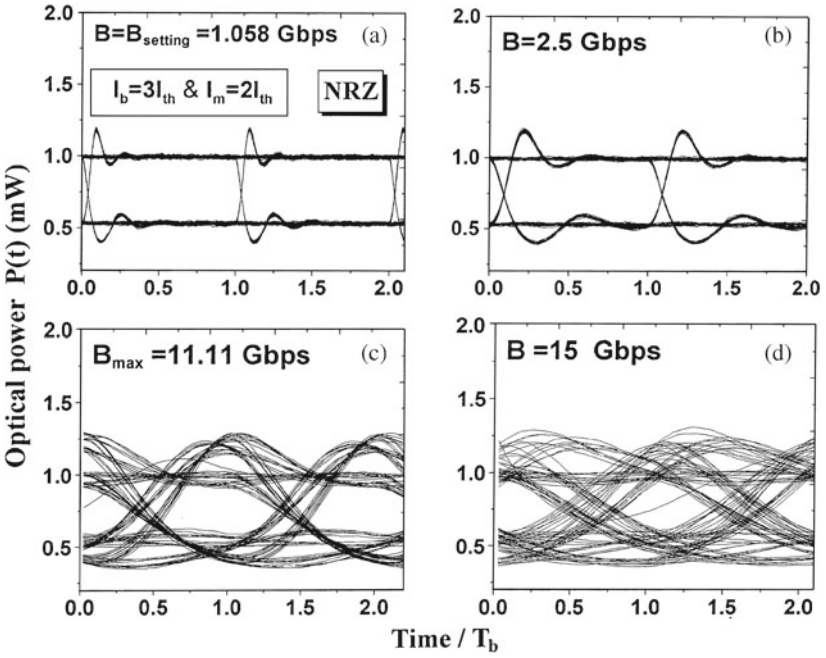

Figure 5. Eye diagrams for NRZ modulation formats when $I_b = 3I_{th}$ and $I_m = 2I_{th}$: (**a**) $B = B_{setting}$, (**b**) $B_{max} > B > B_{setting}$, (**c**) $B = B_{max}$ and (**d**) $B > B_{max}$.

are fixed at 3 and $2I_{th}$, respectively. The values of $B_{setting}$ and B_{max} determined from the laser transients are 1.058 Gbps and $B_{max} = 11.11$ Gbps, respectively. Four values of B are chosen, namely, $B = B_{setting}$, $B_{setting} < B < B_{max}$, $B = B_{max}$ and $B > B_{max}$ to elucidate how the relation of B with both $B_{setting}$ and B_{max} influence digital modulation performance of the semiconductor laser. When $B = B_{setting}$, figure 5a shows that the eye diagram is well open and free from the bit-pattern effects; the rise and fall edges as well as the steady-state '1' and '0' levels are sharp. That is, the modulated laser signal in each '1' bit following '0' bit(s) is the same regardless of the history of these '0' bits. The fluctuations seen at the steady-state power of both logic levels are also manifestation of the quantum noise. The bit-pattern effect is seen in figure 5b in which $B = 2.5$ Gbps $> B_{setting}$, and the bit slot T_b becomes shorter than the setting time $t_{setting}$ of the relaxation oscillations. As seen in the figure, there are different turn-on edges (paths to the '1' level) and bulges-on-top of the eye, which result in partial closure of the eye diagram. These effects enhance as B increases beyond $B_{setting}$. In this case, TOJ increases to 2.75 ps. In figure 5c, B reaches the upper limit of the modulation bit rate B_{max}, which corresponds to a TOJ as strong as 9.05 ps. The eye diagram is almost closed with many turn-on edges and bulges-on-top. When B increases further, as shown in figure 5d, the eye diagram becomes completely closed and the digital modulation performance of the laser deteriorates.

The corresponding eye diagrams under the RZ modulation are shown in figures 6a–d. The width of the eye diagram is one half of that of the NRZ eye diagrams as the bit slot of each '1' bit is set as $T_b/2$. Therefore as seen in the figures, the steady-state '1' level

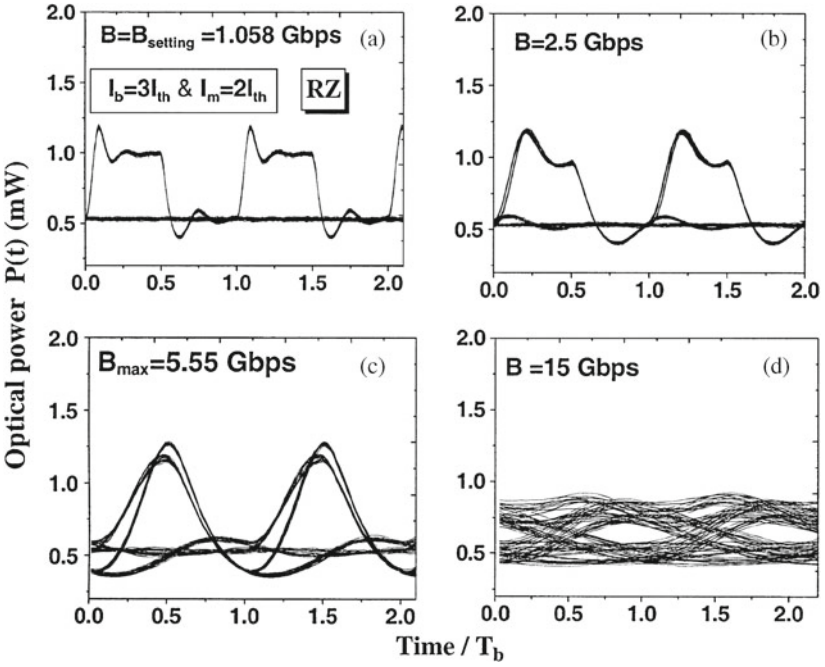

Figure 6. Eye diagrams for RZ modulation formats when $I_b = 3I_{th}$ and $I_m = 2I_{th}$: (**a**) $B = B_{setting}$, (**b**) $B_{max} > B > B_{setting}$, (**c**) $B = B_{max}$ and (**d**) $B > B_{max}$.

nearly disappears because the '1' bit does not continue longer than $T_b/2$. In this case, value of B_{max} is reduced to half under the NRZ modulation. This is reflected in the shown eye diagrams as they exhibit similar behaviour to those under the NRZ modulation with the increase of B. However, the eye diagram is almost closed with many turn-on edges and bulges-on-top at bit rate $B_{max} = 5.55$ Gbps which is one half of that under the NRZ modulation. When B increases further as shown in figure 6d, the eye diagram becomes completely closed and the digital modulation performance of the laser deteriorates. The investigation of the eye diagram characteristics with the increase of B relative to $B_{setting}$ was also reported by Gustavsson *et al* [9] and Ahmed *et al* under NRZ modulation [8].

4.4 *Turn-on jitter (TOJ)*

As inferred from the above discussion, TOJ is a critical property of the laser modulation performance and is a limiting factor to the bit rate. Figures 7a and b plot variations of TOJ with I_m under both the NRZ and RZ modulation formats when $I_b = 1.5$ and $3I_{th}$, respectively. The bit rate $B = 2.5$ Gbps is chosen such that $B_{setting} < B < B_{max}$ over the relevant range of plotted modulation current I_m. Figure 7a shows that TOJ decreases with the increase in I_m, which is due to suppression of the intrinsic intensity noise and improvement of laser coherency with the increase of the modulation current [5]. The overall range of TOJ is 4.88–14.65 ps under the NRZ modulation format, whereas it records 4.75–22.07 ps under the RZ modulation format. The figure shows also that up

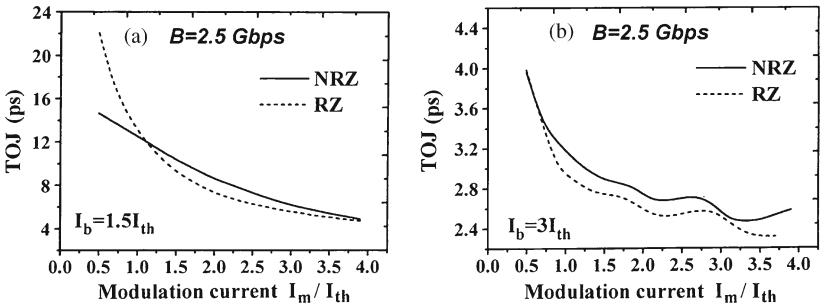

Figure 7. Variation of TOJ with I_m for (**a**) $I_b = 1.5I_{th}$ and (**b**) $I_b = 3I_{th}$ under both RZ and NRZ modulations.

to $I_m = 1.1I_{th}$, the RZ-TOJ values are greater than those of the NRZ-TOJ. Above this modulation current, the RZ-TOJ becomes little smaller than the NRZ-TOJ. According to the analysis by Ahmed *et al* [8], both the intrinsic laser noise and the pseudorandom bit pattern are the main contributors to TOJ. The former contributes significantly at low currents and its effect decreases with the increase in current due to improvement of laser coherency, while the latter effect adds to TOJ when $B_{setting} < B < B_{max}$. Therefore, the results shown in figure 7 indicate that the turn-on delay of the RZ-modulated signal is more sensitive to the intrinsic noise in the low range of modulation current than that of the NRZ-modulated signal. On the other hand, the RZ bit-pattern effect contributes more to the fluctuation of the turn-on delay than under NRZ modulation in which there are different histories of '0' bits preceding the '1' bit(s).

Figure 7b plots variation of TOJ with I_m under the NRZ and RZ modulation formats when $B = 2.5$ Gbps which is lower than B_{max} but higher than $B_{setting}$ over the relevant range of I_m. Similar to the case of $I_b = 1.5I_{th}$, the figure shows that TOJ decreases with the increase in I_m. The overall range of TOJ values is 2.5–3.9 ps under the NRZ modulation format, which is little larger than the range (2.3–3.9 ps) predicted under the RZ modulation format. The results also show that up to $I_m = 0.7I_{th}$, both NRZ-TOJ and RZ-TOJ attain similar values. Above this current level, the RZ-TOJ becomes weaker than the NRZ-TOJ, which indicates that the bit-pattern effect is more enhanced under the NRZ modulation. Similar results were reported in [8]. By comparing these results with those obtained when $I_b = 1.5I_{th}$ in figure 7a, one can find that when $I_m \leq 0.7I_{th}$, the NRZ-TOJ values are higher than that of RZ-TOJ values when $I_b = 1.5I_{th}$, whereas both the NRZ-TOJ and RZ-TOJ attain close values when $I_b = 3I_{th}$. Also, the overall range of TOJ values when $I_b = 1.5I_{th}$ is larger than those when $I_b = 3I_{th}$, which indicates that the TOJ decreases with the increase of I_b.

4.5 *Q-parameter (Q_{signal}) of the modulated laser signal*

In this subsection, influence of the modulation parameters on the eye diagram opening is discussed quantitatively in terms of the Q-factor of the laser signal Q_{signal}. We apply the technique illustrated in §3 to determine the most open section of the eye diagram. At each instant T_d, the average powers $\bar{P}_1$ and $\bar{P}_0$ and the corresponding standard deviations σ_1

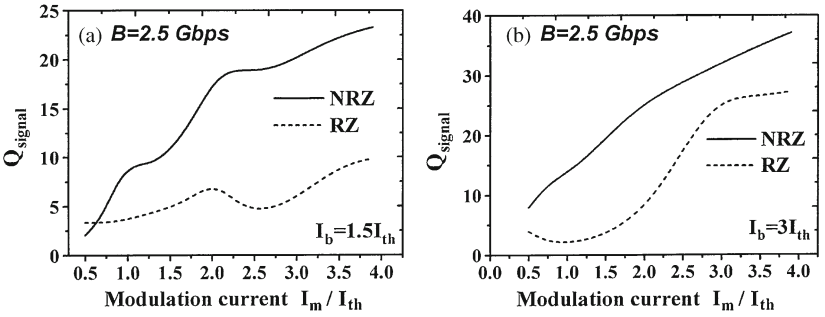

Figure 8. Variation of Q_{signal} with I_{m} for (**a**) $I_{\text{b}} = 1.5I_{\text{th}}$ and (**b**) $I_{\text{b}} = 3I_{\text{th}}$ under both RZ and NRZ modulations.

and σ_0 in the '1' and '0' levels, respectively, are evaluated. These values are then used to calculate Q_{signal} using eq. (21). The results showed that Q_{signal} improves by shifting the decision time T_{d} toward the end of the bit attaining maximum values when $T_{\text{d}} = 0.9T_{\text{b}}$ for the NRZ modulation and $T_{\text{d}} = 0.45T_{\text{b}}$ for the RZ modulation. This far decision point (near the end of the bit) corresponds to the middle of the eye, which is the most open part of the eye diagrams as can be seen in figures 7b and 6b. These results agree with the results predicted by Balle *et al* [17] and Ahmed *et al* [8].

Figures 8a and b show variation of Q_{signal} with I_{m} under both the NRZ and RZ modulation formats when $I_{\text{b}} = 1.5$ and $3I_{\text{th}}$, respectively. The obtained values of Q_{signal} under NRZ format match those obtained by Ahmed *et al* [8]. Figure 8a shows that Q_{signal} increases in general with the increase of I_{m}, which can be interpreted as follows. The increase of I_{m} results in an increase in the average power $\bar{P}_1$ in the '1' level and slight decrease in the average power $\bar{P}_0$ in the '0' level, which then enlarges the numerator $(\bar{P}_1 - \bar{P}_0)$ of eq. (21). The power fluctuations in both '1' and '0' levels are simultaneously suppressed due to the improvement of laser coherency [4], which then contributes to the decrease in the denominator $(\sigma_1 + \sigma_0)$. The net result is the increase of Q_{signal} with the increase of I_{m}. The figure shows that when $I_{\text{m}} > 0.6I_{\text{th}}$, the Q_{signal} values under the NRZ format are larger than those under the RZ format. That is, the eye diagram is more open and the modulation characteristics are better under the NRZ format over the entire range of I_{m}. Similar to the case of $I_{\text{b}} = 1.5I_{\text{th}}$, figure 8b shows that Q_{signal} increases in general with the increase of I_{m}. The Q_{signal} values in this case are larger than those when $I_{\text{b}} = 1.5I_{\text{th}}$, which indicates that Q_{signal} increases with the increase of I_{b}. These results confirm again the improvement of modulation performance with the increase of I_{b} and/or I_{m}.

5. Conclusions

We introduced simulation of the semiconductor laser dynamics under RZ and NRZ pseudorandom modulation. The simulation was based on numerical large-signal analysis of the stochastic laser rate equations. Approximated estimates of the maximum modulation bit rate and setting bit rate at each modulation condition were given. The modulation

performance was evaluated in terms of the laser signal, frequency chirp, eye diagram and TOJ. Based on the obtained results, the following conclusions can be traced:

(1) The peak-to-peak frequency chirp increases with the increase of the modulation current under both RZ and NRZ formats. It decreases remarkably with the increase of the bias current, and saturates at 8.6 GHz when the bias current increases beyond $2.5I_{\text{th}}$. The chirp is higher under the RZ modulation format than under the NRZ modulation format, which indicates that the NRZ scheme has a better defined central frequency compared to the RZ scheme.
(2) When the modulation bit rate is higher than the setting bit rate of the relaxation oscillation, the laser exhibits enhanced TOJ and the eye diagram is partially closed. TOJ decreases with the increase of the bias and/or modulation current for both formats of modulation.
(3) The TOJ values under NRZ modulation is lower than those under RZ modulation when $I_{\text{b}} = 1.5I_{\text{th}}$, but are larger when $I_{\text{b}} = 3I_{\text{th}}$. That is, under high speed modulation, the RZ format yields better digital modulation performance near the threshold level, whereas the NRZ format is more preferable far above the threshold.
(4) The Q-factor of the laser signal increases with the increase of the bias and/or modulation current attaining larger values under the NRZ modulation format than those under the RZ modulation format, which indicates that the eye diagram is more open under the NRZ format than under the RZ format.

References

[1] K Petermann, *Laser diode modulation and noise* (Kluwer Academic, Dordrecht, 1988)
[2] M Ahmed, *Pramana – J. Phys*. **71**, 90 (2008)
[3] G P Agrawal, *IEEE J. Quantum Electron*. **26**, 1901 (1990)
[4] G P Agrawal and N K Dutta, *Semiconductor lasers* (Van Nostrand Reinhold, New York, 1993)
[5] M Ahmed, M Yamada and M Saito, *IEEE J. Quantum Electron*. **37**, 1600 (2001)
[6] L Zei, K Obermann, T Czogalla and K Petermann, *IEEE Photon. Technol. Lett*. **11**, 6 (1999)
[7] G P Agrawal, *Optical fiber communication systems* (Van Nostrand Reinhold, New York, 2003)
[8] M Ahmed, M Yamada and S W Z Mahmoud, *J. Appl. Phys*. **101**, 3119 (2007)
[9] J S Gustavsson, A Haglund, J Bengtsson and A Lasrsson, *IEEE J. Quantum Electron*. **38**, 1089 (2002)
[10] S W Z Mahmoud, M Ahmed, K Abdelhady and A Mahmoud, *Proc. Nat. Radio Sci. Conf. Cairo* D08 (2009)
[11] M Ahmed, *J. Phys*. **D42**, 185104 (2009)
[12] C Laverdière, A Fekecs and M Tetu, *IEEE Photon. Technol. Lett*. **15**, 446 (2003)
[13] K Sato, S Kuwahara and Y Miyamoto, *IEEE J. Quantum Electron*. **23**, 3790 (2005)
[14] S W Z Mahmoud, *Egypt. J. Solids* **30**, 237 (2007)
[15] V Bobrovs, J Porins and G Ivanovs, *Electron. Electr. Engin*. **76**, 55 (2007)
[16] A Yin, L Li and X Zhang, *Opt. Int. J. Light Electron*. **2**, 1550 (2009)
[17] S Balle, M Homar and M S Miguel, *IEEE J. Quantum Electron*. **31**, 1401 (1995)
[18] D Liu, L Wang and J He, *J. Lightwave Technol*. **28**, 3128 (2010)
[19] M Yamada and Y Suematsu, *J. Appl. Phys*. **52**, 2653 (1981)
[20] R L Burden, J D Faires and A C Reynolds, *Numerical analysis* (Prindle, Weber and Schmidt, Boston, 1981)